A First-Principles Study of (*R*)- and (*S*)-PPA Molecules on Cu(111)

Bing Dai,[†] Jinlong Yang,*[,†,‡] J. G. Hou,[†] and Qingshi Zhu[†,‡]

Hefei National Laboratory for Physical Sciences at Microscale, University of Science and Technology of China, Hefei, Anhui 230026, People's Republic of China, USTC Shanghai Institute for Advanced Studies, University of Science and Technology of China, Shanghai 201315, People's Republic of China

Received: June 20, 2004; In Final Form: February 3, 2005

The adsorption of (*R*)- and (*S*)-2-phenylpropionamide (PPA, $C_9H_{11}ON$) molecules on a Cu(111) surface has been investigated using the density functional method with supercell models. The adsorption orientations of both (*R*)- and (*S*)-PPA molecules on the surface are the same: the phenyl rings are approximately parallel to the Cu(111) surface and positioned in the hollow sites, the amino and methyl groups occupy two-bridge sites, and the carbonyl occupies the top site. After the adsorption, the bond lengths in the two enantiomers are almost unchanged, but the changes for two dihedral angles show differences, especially for (*R*)-PPA molecule. The first angles between the (N,C9,C7) plane and the (C9,C7,C6) plane are 19.4 and 0.7° for (*R*)- and (*S*)-PPA molecules, respectively, and the second angles between the (C8,C7,C6) plane and the (C7,C6,-C5) plane are 74.8 and 0.4° for (*R*)- and (*S*)-PPA molecules, respectively. The adsorption energies of (*R*)- and (*S*)-PPA molecules are calculated to be −34 and −26 kJ mol^{-1}, respectively. The simulated scanning tunneling microscopy (STM) images of (*R*)- and (*S*)-PPA molecules on the Cu(111) surface display different features and are coincident with the experimental ones. The interaction between the adsorption molecule and the metal surface is found to be responsible for the discrimination of (*R*)- and (*S*)-PPA molecules on the surface.

Introduction

Chirality is a fundamental aspect of chemical biology and is of central importance in pharmacology. Along with the development of chemical and pharmaceutical industries, the enantiomerically pure compounds are more and more demanded, which request a precise control over a chemical reaction by the direction of its enantioselectivity.[1] Therefore, the methods of chiral discrimination become very important. Besides the traditional optical methods to discriminate these enantiomers, recently, there have been many successful applications of chemical force microscopy (CFM) and scanning tunneling microscopy (STM) to measure the conformation and chirality of individual molecules on metal or semiconductor surfaces under ambient, ultrahigh vacuum, or electrochemical conditions.[2−12] For example, McKendry et al.[2] distinguished the two enantiomers of mandelic acid arrayed on a surface using chiral molecules attached to the probe tip, through differences in both the adhesion forces and the frictional forces measured by the probe with CFM. Ohtani et al.[3] observed the STM images of two-dimensional chirality of an atropisomeric compound, (*R*)- and (*S*)-1,1′-binaphthalene-2,2′-dithiol (BNSH), anchored covalently on a Au(111) surface. The (*R*)- and (*S*)-BNSH molecules are discriminated by the different lattice patterns induced by the arrangement of naphthalene moieties of the BNSH molecule with two twisted aryl groups. Lorenzo et al.[5] investigated the adsorption of tartaric acid molecules on a Cu(110) surface and their bestowal of the chirality to the modified surface with STM. The intermolecular hydrogen-bonding interactions of the α-hydroxy groups indicate the different directions of long chain growth for the (*R*)- and (*S*)-tartaric acid molecules in the spatial alignment, which make the chirality discriminable. Messina et al.[8] acquired the STM images of chiral complexes generated by the assembly of achiral components, 1,3,5-tricarboxylic benzoic acid (trimesic acid, TMA), and a metal center, Fe atom, at a Cu(100) surface at the single molecular level. They found that the chiral complexes can be stabilized by metal−ligand interactions, and the high-resolution STM images with intracomplex features can discriminate the chirality successfully.

Despite many important experimental investigations, the first-principles studies of the adsorption of chiral molecules on surfaces are far from completeness. Barbosa et al.[13] studied the interactions of different bitartrate isomers on a Cu(110) surface with the periodic density functional theory (DFT) and showed that the (*R*,*R*- or *S*,*S*-) domains are formed by the formation of optimal intramolecular hydrogen bonds in the chemisorption structures. More recently, Barbosa et al.[14] investigated the role of pyroglutamic acid as a chiral auxiliary in the hydrogenation of *o*-toluic acid and 2-methylnicotinic acid on the Rh(111) surface by using periodic DFT. They found that it is effective to use the chiral auxiliaries for the enantioselective hydrogenation of specific target molecules, and the different functional groups in the target molecule could lead to a reduction of diastereomeric excess. They also demonstrated that different enantioselectivity can be attained due to adsorbate−substrate interactions. Besides the first-principles calculations, the effect of the formation of chiral templates on the enantioselectivity of model heterogeneous catalysts was studied theoretically in the framework of a cooperative sequential adsorption model.[15]

In most of the above-mentioned studies, the mechanisms for chiral discriminations are based on the interactions of intermolecules or intramolecules, which cause different lattices, different adsorption orientations, and so forth. Recently, some experimental works[9−12] also indicate that the discrimination

* Corresponding author. E-mail: jlyang@ustc.edu.cn.
† Hefei National Laboratory for Physical Sciences at Microscale.
‡ USTC Shanghai Institute for Advanced Studies.

10.1021/jp047319g CCC: $30.25
Published on Web 04/02/2005

mechanism of chiral molecules on surfaces may be based on the molecule−substrate interactions. For examples, Fasel et al.[9] illuminated experimentally that the mechanism of chiral transfer from helical heptahelicene molecules ($C_{30}H_{18}$) into the close-packed monomolecular layer on a Cu(111) surface is not only governed by the lateral interactions between the molecules but is also influenced by the molecule−substrate interactions. Xu et al.[10] discriminated the (*R*)- and (*S*-)-2-phenylpropionamide (PPA, $C_9H_{11}ON$) molecules on a Cu(111) surface in 0.1 M $HClO_4$ using electrochemical STM (ECSTM). Although the two enantiomers form the same lattices on the surface, their features in the STM images of single molecules are different from each other. So far, there have been few theoretical studies to explore the discrimination mechanism mainly based on molecule−substrate interactions.

In the present paper, we investigate the interactions of (*R*)- and (*S*)-PPA molecules on a Cu(111) surface. More insights about the formation and stability of the two enantiomers on the metal surface have been uncovered with ab initio DFT calculations in *k* space with periodic boundary conditions. Our calculations interpret the experimental phenomena[10] and illuminate that the mechanism of discrimination of these two enantiomers is based on the interactions between the adsorption molecules and the metal surface. This kind of mechanism may be applied to discriminate the enantiomers at the single molecular level.

Computational Details

Our periodic DFT calculations are performed on the basis of the linear combination of atomic orbital and molecular orbital (LCAO-MO) method. The atomic orbitals are represented by a double-numeric quality basis set with d-polarization functions (DND)[16] with density functional semicore pseudopotential corrections.[17] In this work, the generalized gradient approximation (GGA) to the DFT is employed, with the Perdew−Burke−Ernzerhof (PBE) correlation energy.[18] PBE has generally good performance for a variety of properties, including van der Waals forces,[19] and it has been concluded as good for van der Waals forces in a comment.[20] PBE also achieves an accuracy similar to the second-order Moller−Plesset (MP2) method for some systems, such as the benzene−ammonia complex.[21] For the rare gas dimer, a weak interaction system, PBE is also the best functional.[22] Thus, in the paper, we employed PBE to calculate the adsorption of PPA molecules on a Cu(111) surface. Spin-restricted wave functions are employed. All calculations are carried out using the molecular simulation package DMol^3.[16]

Experimentally, both (*R*)- and (*S*)-PPA molecules adsorb on a Cu(111) surface in the same (4×4) superlattice.[10] We use a periodic three-layer slab with a (*R*)- or (*S*)-PPA molecule on one side of the slab, a 70-atom unit cell of $C_9H_{11}ONCu_{48}$ with periodic boundary conditions to model the adsorption system. Test calculations show that the adsorption energy of one of the systems does not change significantly by using three- or four-metal-slab models. In the *xy* plane, we choose a (4×4) supercell, which corresponds to 16 Cu atoms per metal layer and one PPA molecule in the unit cell. The slab is separated from its periodic image in the *z* direction by a vacuum space, 21.55 Å for both (*R*)- and (*S*)-PPA molecular adsorption models, which is wide enough to make sure no interactions exist among slabs and PPA molecules in different unit cells. To reduce the effect of the stress by the use of the slab model, an optimized bulk Cu−Cu distance, 2.56 Å, is used, which is just the same as the experimental one.[24] The models we used are shown in Figure 1.

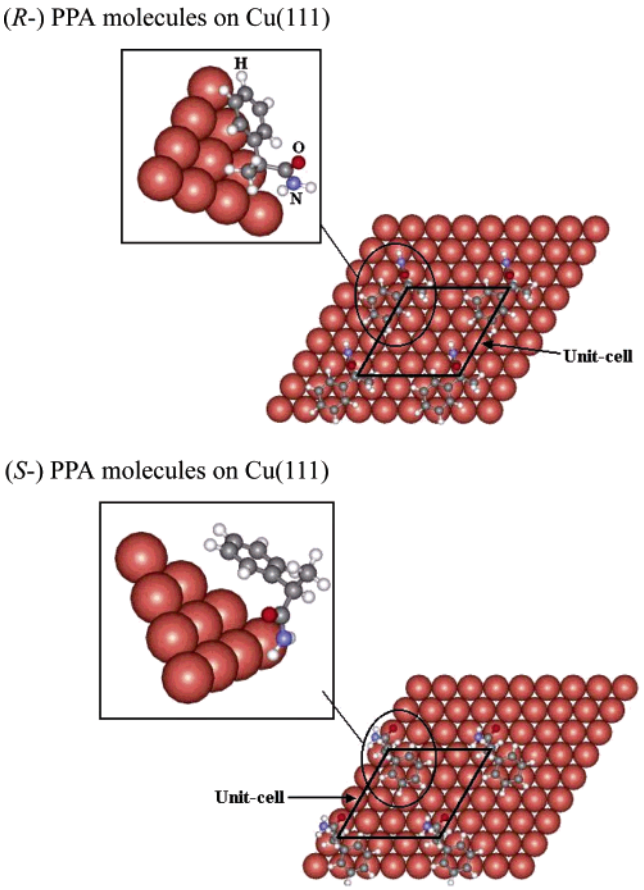

Figure 1. Computational models and the unit cells of (*R*)- and (*S*)-PPA molecules on Cu(111).

During the structural optimizations, we fix the Cu atoms in the second and third layers in their bulk configurations and allow the Cu atoms in the first layer and PPA molecule in the supercell to move until all forces vanished within 1.0×10^{-3} hartrees per bohr. Several initial configurations are chosen to find the final optimized one. The Brillouin-zone integrations have been performed on a $2 \times 2 \times 1$ Monkhorst−Pack grid of K-points for all structures, which allows convergence to be reached for the calculated energy.

Results and Discussion

The optimized structures of (*R*)- and (*S*)-PPA molecules in the gas phase are shown in Figure 2. A phenyl ring, methyl, and $CONH_2$ groups compose a PPA molecule. The chiral feature of PPA molecules arises from the arrangement of methyl and $CONH_2$ groups. The chiral centers in the molecules are indicated by arrows.

In experiments, both (*R*)- and (*S*)-PPA adlayers have the same adsorption behaviors of the chiral molecules at the liquid/solid interface.[10] Although Cu(111) is not a chiral surface, the chiral nature of the molecules makes the discrimination possible. The optimized structures of (*R*)- and (*S*)-PPA molecules on the Cu-(111) surface are shown in Figure 3. The chirality is clearly seen from the arrangement of the methyl and $CONH_2$ groups. When PPA molecules adsorb on the surface, the phenyl ring has three kinds of adsorption sites: top, bridge, and hollow sites. Though the total energies of the three kinds of sites are almost the same, the hollow sites do have the lowest ones for both (*R*)- and (*S*)-PPA molecules according to our calculations, which are about 1 kJ mol^{-1} lower than the other two. From Figure 3, the adsorption modes of PPA molecules can be viewed as that

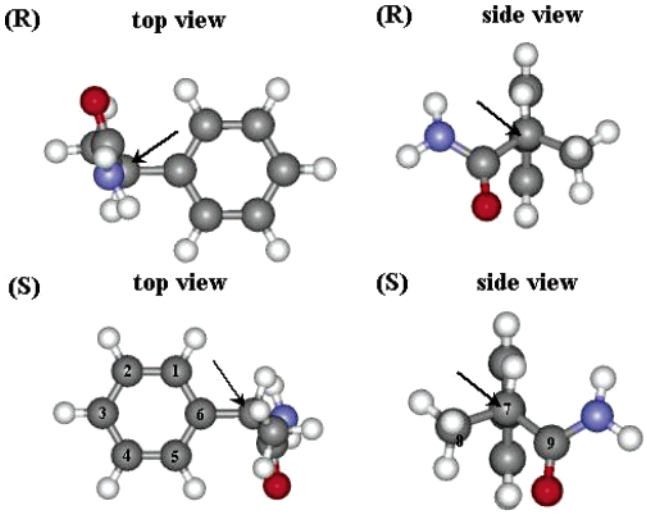

Figure 2. Optimized structures of (*R*)- and (*S*)-PPA molecules in the gas phase.

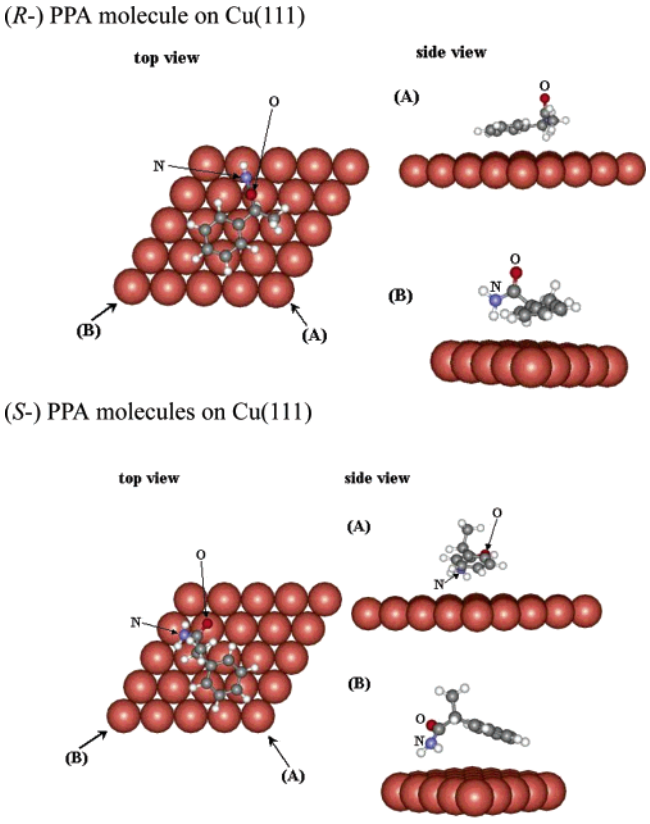

Figure 3. Optimized structures of (*R*)- and (*S*)-PPA molecules adsorbed on the Cu(111) surface.

the (*R*)-PPA molecule adsorbs via the phenyl ring, while the (*S*)-PPA molecule adsorbs via the NH_2 function of the amide group. The adsorption orientations of both (*R*)- and (*S*)-PPA molecules on the surface are the same: the phenyl rings are approximately parallel to the Cu(111) surface and positioned in the hollow sites, the amino and methyl groups occupy two-bridge sites, and the carbonyl occupies the top site. The adsorption orientations are the same as the experimental ones.[10] Compared with the structures in the gas phase, the methyl and $CONH_2$ groups of PPA molecules rotate around the C6−C7 axes for an angle when PPA molecules are adsorbed on the copper surface. The rotation angle of the (*R*)-PPA molecule is larger than that of the (*S*)-PPA one.

TABLE 1: Bond Lengths (Values in Å) and Dihedral Angles of (*R*)- and (*S*)-PPA Molecules in the Gas Phase and after the Adsorption

	S		*R*	
	gas	adsorption	gas	adsorption
C−O	1.229	1.231	1.229	1.229
C−N	1.372	1.369	1.375	1.368
C7−C9	1.539	1.539	1.540	1.544
C7−C8	1.536	1.537	1.533	1.530
C6−C7	1.524	1.523	1.524	1.525
C5−C6	1.405	1.406	1.406	1.404
C1−C6	1.405	1.405	1.404	1.409
C4−C5	1.398	1.398	1.398	1.402
C3−C4	1.401	1.402	1.400	1.398
C2−C3	1.398	1.399	1.399	1.402
C1−C2	1.400	1.400	1.399	1.399
D(N,C9,C7,C6)	96.2°	96.9°	−84.5°	−103.9°
D(C8,C7,C6,C5)	−70.4°	−70.0°	66.9°	−7.9°

Table 1 lists the bond lengths and dihedral angles of (*R*)- and (*S*)-PPA molecules in the gas phase and after the adsorption. The distances between the phenyl rings and the copper surface are about 3.5 and 4.0 Å for (*R*)- and (*S*)-PPA molecules, respectively. The changes of the bond lengths of PPA molecules are tiny after the adsorption, indicating that the interactions between the PPA molecules and the copper surface are very weak and the PPA molecules do not have a corrosive chemisorption on the surface. The main reason the PPA molecules mainly keep their stable structures of the gas phase is that no molecular hydrogen has been dissociated and no hydrogen atom is present on the surface. However, the changes for two dihedral angles show differences, the first angles between the (N,C9,-C7) plane and the (C9,C7,C6) plane are 19.4 and 0.7° for (*R*)- and (*S*)-PPA molecules, respectively, and the second angles between the (C8,C7,C6) plane and the (C7,C6,C5) plane are 74.8 and 0.4° for (*R*)- and (*S*)-PPA molecules, respectively. The adsorption of (*R*)-PPA molecules is stronger than that of (*S*)-PPA ones. The weak adsorption of PPA molecules on a copper surface testifies that our approximate fixing of the surface atoms is reasonable.

To understand the stabilities of the adsorption of (*R*)- and (*S*)-PPA molecules on a Cu(111) surface in more detail, we have performed a comparison of their adsorption energies. The adsorption energy is calculated as the energy difference between the initial system (the gas phase molecules and the clean surface) and the final adsorption configuration. The values are −34 and −26 kJ mol^{-1} for (*R*)- and (*S*)-PPA molecules, respectively, as shown in Figure 4.

The adsorption energies of (*R*)- and (*S*)-PPA molecules on a Cu(111) surface with two different modes (that is, the *R* isomer with the orientation via the NH_2 function of the amide group and the *S* isomer via the phenyl ring) are listed in Table 2, which shows that the adsorption orientations we chose are energy favorable.

The adsorption process can be decomposed to three distinct elementary steps:[13] (1) molecular deformation, corresponding to the change of the molecular structure in the gas phase to the one found on the surface; (2) molecular arrangement, corresponding to the arrangement of the already deformed molecules with the adsorption domain; (3) molecular interaction with the surface, corresponding to the adsorption of the deformed and arranged molecules assembly onto the surface. The detailed adsorption situations can be found in Figure 4.

The deformed energies are 12 and 1 kJ mol^{-1} for (*R*)- and (*S*)-PPA molecules, respectively. The larger deformed energy of the (*R*)-PPA molecule is consonant with its larger structural

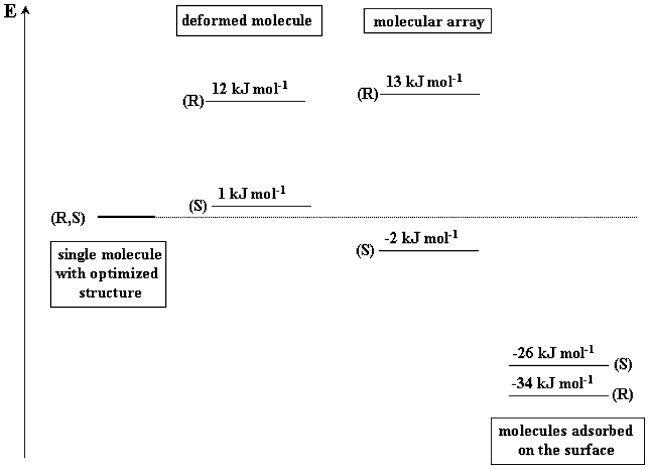

Figure 4. Energy diagram of the (*R*)- and (*S*)-PPA molecules adsorbed on the Cu(111) surface.

TABLE 2: Adsorption Energies of (*R*)- and (*S*)-PPA Molecules on a Cu(111) Surface with Two Different Modes (Values in kJ mol^{-1})

	via the NH_2 group	via the phenyl ring
(*R*)-PPA	−19	−34
(*S*)-PPA	−26	−19

change. The arrangement energies are very small for both (*R*)- and (*S*)-PPA molecules, which are 1 and −3 kJ mol^{-1} for (*R*)- and (*S*)-PPA molecules, respectively. These illuminate that the experimental coverage densities of PPA molecules are not crowded, and the interactions among PPA molecules are very weak. The calculated interaction energies between (*R*)- and (*S*)-PPA molecules and the surface are −47 and −24 kJ mol^{-1}, respectively. The results are consistent with our former discussion of structural changes after the adsorption. Since the changes of bond lengths are tiny for both (*R*)- and (*S*)-PPA molecules, the larger interaction energy of (*R*)-PPA molecules comes mainly from the torsion of the two dihedral angles. One is between the (N,C9,C7) plane and the (C9,C7,C6) plane, and the other is between the (C8,C7,C6) plane and the (C7,C6,C5) plane.

We simulated the STM images for both (*R*)- and (*S*)-PPA molecules on a Cu(111) surface using the Tersoff and Hamann theory.[23] In this method, the tunneling current in the STM can be expressed as

$$I(V) \propto \int_{E_f}^{E_f+eV} \mathrm{d}E\, \rho(\mathbf{r}, E) \quad (1)$$

$$\rho(\mathbf{r}, E) = \sum_i |\psi_i(\mathbf{r})|^2 \delta(E - E_i) \quad (2)$$

where $\rho(\mathbf{r}, E)$, $\psi_i(\mathbf{r})$, E_f, and V are the local density of states of the sample, the sample wave function with energy E_i, the Fermi energy, and the sample bias voltage, respectively. Figure 5 shows the simulated STM images with (*R*)- and (*S*)-PPA molecules on a Cu(111) surface.

Because of the complicated molecular structures of PPA molecules, the experimental STM images are not as clear as the ones of small molecules even for high-resolution images. However, our simulated STM images do present the main features, a circle ring and a "Y" shape tail, of the experimental ones for either of the two images. "M" and "N" denote the methyl and $CONH_2$ groups, respectively. The molecular chirality is directly expressed in the STM images by the arrangement of the methyl and $CONH_2$ groups. Both the distances between the center of the amino group and the chiral center and between the center of the methyl group and the chiral center are close to the distances in the molecules.

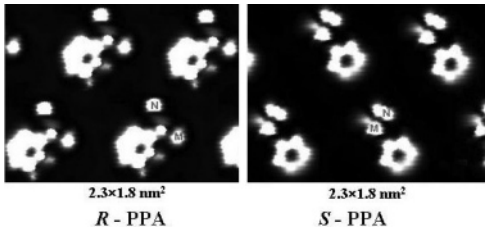

Figure 5. Simulated STM images of the (*R*)- and (*S*)-PPA molecules on Cu(111).

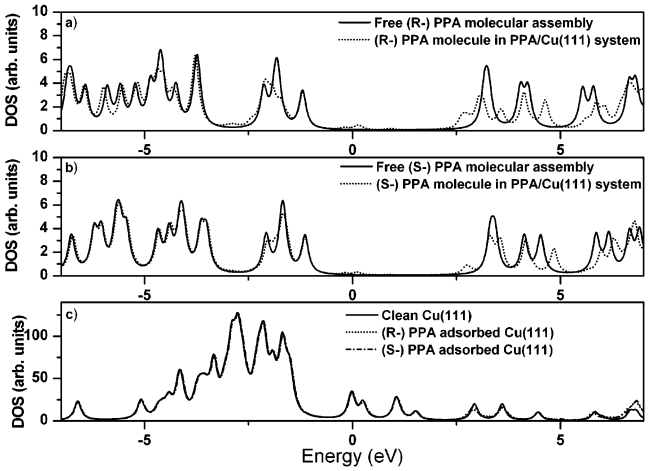

Figure 6. DOS of (a) a free and adsorbing (*R*)-PPA molecular assembly, (b) a free and adsorbing (*S*)-PPA molecular assembly, and (c) Cu(111) with and without PPA molecule. The zero of energy is set as the Fermi energy level of the PPA/Cu(111) system. The DOS of the free (*R*)- and (*S*)-PPA molecular assemblies are shifted to make the location of the first peak below the Fermi energy level repeat that of the PPA/Cu(111) system.

The molecule−substrate interactions are so weak that they do not change dramatically the electronic structure of both (*R*)- and (*S*)-PPA molecules after they are adsorbed on the surface. To demonstrate this explicitly, we plot the density of states (DOS) of the separate surface and molecular assembly as compared with the DOS of the absorbed molecule/surface system in Figure 6. The main effect of the weak interactions is the change of the molecular structure of PPA molecules, and the differences of STM images of (*R*)- and (*S*)-PPA molecules mainly come from the structural changes.

According to both our calculations and the experimental effort,[10] the chirality can be discriminated by STM or ECSTM assuredly. It is concluded that the discrimination mechanism based on molecule−substrate interactions does exist, and a new discrimination technology is probably available. However, the substrate material plays an important role in molecular adsorption;[10] systematic theoretical and experimental studies of the chirality on other substrates are necessary.

Summary

In the present work, the interactions and optimized structures of (*R*)- and (*S*)-PPA molecules on a Cu(111) surface have been investigated systematically with the ab initio DFT in *k* space with periodic boundary conditions. The adsorption orientations of both (*R*)- and (*S*)-PPA molecules on the surface are the same: the phenyl rings are approximately parallel to the Cu(111) surface and positioned in the hollow sites, the amino and

methyl groups occupy two-bridge sites, and the carbonyl occupies the top site. The adsorption energies are −34 and −26 kJ mol^{-1} for (*R*)- and (*S*)-PPA molecules on a Cu(111) surface, respectively. The exiguous bond length distortions and the small adsorption energies illuminate the weak adsorption of both PPA molecules on a Cu(111) surface, though the changes of the dihedral angles between the (N,C9,C7) plane and the (C9,C7,-C6) plane and between the (C8,C7,C6) plane and the (C7,C6,-C5) plane of the (*R*)-PPA molecule are larger than those of the (*S*)-PPA one. To get more information about the adsorption behaviors of PPA molecules, three distinct elementary steps of the adsorption process are calculated: molecular deformation, molecular arrangement, and molecular interaction with the surface. The interaction energies of (*R*)- and (*S*)-PPA molecules are −47 and −24 kJ mol^{-1}, respectively. STM images of (*R*)- and (*S*)-PPA molecules on a Cu(111) surface are simulated using the Tersoff and Hamann theory.[23] The main features of the experimental images are shown, and the molecular chirality can be discriminated from the images. The discrimination mechanism of (*R*)- and (*S*)-PPA molecules on a Cu(111) surface is based on the interactions between the adsorption molecules and the metal surface.

Acknowledgment. We thank professors Lijun Wan and Xi Xu for helpful discussions. This work is partially supported by the National Project for the Development of Key Fundamental Sciences in China (G1999075305 and G2001CB3095), by the National Natural Science Foundation of China (50121202, 20025309, and 10474087), by the USTC-HP HPC project, and by the EDF of USTC-SIAS.

References and Notes

(1) Brown, J. M.; Davies, S. G. *Nature* **1989**, *342*, 631.
(2) McKendry, R.; Theoclitou, M. E.; Rayment, T.; Abell, C. *Nature* **1998**, *391*, 566.
(3) Ohtani, B.; Shintani, A.; Uosaki, K. *J. Am. Chem. Soc.* **1999**, *121*, 6515.
(4) Böhringer, M.; Schneider, W. D.; Berndt, R. *Angew. Chem., Int. Ed.* **2000**, *39*, 792.
(5) Lorenzo, M. O.; Baddeley, C. J.; Muryn, C.; Raval, R. *Nature* **2000**, *404*, 376.
(6) Schunack, M.; Lægsgaard, E.; Stensgaard, I.; Johannsen, I.; Besenbacher, F. *Angew. Chem., Int. Ed.* **2001**, *40*, 2623.
(7) Feyter, S. D.; Gesquière, A.; Wurst, K.; Amabilino, D. B.; Veciana, J.; Schryver, F. C. D. *Angew. Chem., Int. Ed.* **2001**, *40*, 3217.
(8) Messina, P.; Dmitriev, A.; Lin, N.; Spillmann, H.; Abel, M.; Barth, J. V.; Kern, K. *J. Am. Chem. Soc.* **2002**, *124*, 14000.
(9) Fasel, R.; Parschau, M.; Ernst, K.-H. *Angew. Chem., Int. Ed.* **2003**, *42*, 5178.
(10) Xu, Q. M.; Wang, D.; Wan, L. J.; Wang, C.; Bai, C. L.; Feng, G. Q.; Wang, M. X. *Angew. Chem., Int. Ed.* **2002**, *41*, 3408.
(11) McFadden, C. F.; Cremer, P. S.; Gellman, A. J. *Langmuir* **1996**, *12*, 2483.
(12) Ahmadi, A.; Attard, G.; Feliu, J.; Rodes, A. *Langmuir* **1999**, *15*, 2420.
(13) Barbosa, L. A. M. M.; Sautet, P. *J. Am. Chem. Soc.* **2001**, *123*, 6639.
(14) Barbosa, L. A. M. M.; Sautet, P. *J. Catal.* **2003**, *217*, 23.
(15) Roma, F.; Zgrablich, G.; Stacchiola, D.; Tysoe, W. T. *J. Chem. Phys.* **2003**, *118*, 6030.
(16) (a) Delley, B. *J. Chem. Phys.* **2000**, *113*, 7756. (b) Delley, B. *J. Chem. Phys.* **1990**, *92*, 508.
(17) Hamann, D. R.; Schluter, M.; Chiang, C. *Phys. Rev. Lett.* **1979**, *43*, 1494.
(18) Perdew, J. P.; Burke, K.; Ernzerhof, M. *Phys. Rev. Lett.* **1996**, *77*, 3865.
(19) Perdew, J. P.; Burke, K.; Ernzerhof, M. *Phys. Rev. Lett.* **1998**, *80*, 891.
(20) Wesolowski, T. A. *J. Chem. Phys.* **2000**, *113*, 1666.
(21) Enkvist, C.; Zhang, Y. K.; Yang, W. T. *Int. J. Quantum Chem.* **2000**, *79*, 325.
(22) Zhang, Y. K.; Pan, W.; Yang, W. T. *J. Chem. Phys.* **1997**, *107*, 7921.
(23) Tersoff, J.; Hamann, D. *Phys. Rev. Lett.* **1983**, *50*, 1998.
(24) Straumanis, M. E.; Yu, L. S. *Acta Crystallogr.* **1969**, *25A*, 676.